140–220-GHz DHBT Detectors

Vessen Vassilev, Herbert Zirath, *Fellow, IEEE*, Rumen Kozhuharov, and Szhau Lai, *Student Member, IEEE*

***Abstract*—This paper discusses G-band (140–220 GHz) detectors based on a 250-nm InP–InGaAs–InP double heterojunction bipolar transistor process available from the Teledyne Scientific Company. Two types of detectors are presented—a passive detector where the transistor's base-emitter junction nonlinearity is used, and an active detector, where the transistor transconductance nonlinearity is used for detection. Measurements of transistor noise-power spectrum density at low frequencies is used to model and predict the noise equivalent power (NEP) of the detectors. Analysis of responsivity and noise is presented and compared with measurements. Both configurations are analyzed and compared in terms of noise-voltage, responsivity and NEP. The conclusion that the passive detector offers lower NEP is analyzed and explained.**

***Index Terms*—Double heterojunction bipolar transistor (DHBT), flicker noise, G-band, InP, monolithic microwave integrated circuit (MIMIC), noise equivalent power (NEP), passive imaging, power detectors, radiometers, receivers, remote sensing, responsivity.**

I. Introduction

APPLICATIONS such as imaging and atmospheric studies require sensitive power detectors. Real-time imaging systems require multipixel receivers. Within security imaging, there is an obvious need for cheaper and more compact front-ends that would allow introducing real-time scanning systems at a reasonable price. Passive systems working around 94 GHz are available today and are based on a low-noise amplifier (LNA) followed by a power detector [1]–[4]. The low-noise detector technologies available today include zero-bias Schottky [5]–[7] and tunnel diodes [7], [9] [however, tunnel diodes are not commercially available above W-band (above 110 GHz)], and Schottky power-detectors, although expensive, are available with high responsivity and low-noise. Other technologies demonstrating detectors at millimeter-wave (mm-wave) and sub-mm-wave frequencies include SiGe BiCMOS [10], Si, and GaAs field-effect transistors [11], [12]. The last two technologies are particularly suitable for active, multipixel inexpensive terahertz imaging cameras.

To achieve better spatial resolution and more compact scanners, moving up in frequency above 100 GHz is required. Compact and cheaper front-ends require technology where an LNA is integrated with a power detector. Such solutions require the use of double heterojunction bipolar transistor (DHBT) or high-electron mobility transistor (HEMT) processes to make a sensitive detector that is integrated on the same monolithic microwave integrated circuit (MMIC) as the LNA. Neither Schottky nor tunnel diodes are suitable for integration with existing low-noise HEMT or HBT technologies. Examples of such front ends at W-band using a commercial SiGe process can be found in [2], [3], and [4]. The drawback of this solution is the need for biasing, which implies increased low-frequency noise and requires good quality biasing sources. Usually, LNA-power detector circuits are designed in such a way that the output level after the LNA is just below the saturation level for the detector, typically -30 to -40 dBm. It is obvious that, even for zero-bias detectors pumped at RF power close to saturation, $1/f$ noise is present.

This paper presents two types of detectors: a passive type where the base-emitter junction nonlinearity of a 0.25×2 μm DHBT is used for detection, while the collector port is left open, and an active type where the DHBT is biased at the collector port. An important figure of merit for a detector is its voltage responsivity (R_V) and video noise voltage (Vn).

Section II presents a method based on the polynomial expansion of the current–voltage characteristic (IVC) giving the upper limit on R_V, providing a perfect and lossless match [13]. This method is modified for the case of the active detector and is used to calculate and compare the achievable responsivity of both types of detectors. Using this analysis, Section VII shows why the passive detector delivers lower noise equivalent power (NEP) than the active. In addition, a harmonic balance (HB) simulation is used to confirm the theoretically derived values for the responsivity. This responsivity is compared with measurements in Sections IV and V.

Section III gives a brief overview of the DHBT process. The transistor model implemented in the design kit does not include low-frequency noise. To be able to predict the NEP at video frequencies, measurements of the transistor noise-power spectrum density are performed to extract the flicker noise coefficients. A simple way to include the low-frequency noise into the transistor model is presented in Sections IV and V. The calculated noise voltages are compared with the noise-voltage measurements at the video output and estimates of the NEP of both detectors is given.

Compared with a passive detector, the active circuit produces $\sqrt{\beta}$ times higher noise voltage, but it cannot deliver the expected β times higher voltage responsivity. The reason for this is explained in Section VII.

Section VIII discusses the temperature resolution achievable by the detectors and its relation to the NEP and video bandwidth. The measured NEP of the detectors is compared with the NEP of detectors based on SiGe technology.

Manuscript received October 08, 2012; revised April 10, 2013; accepted April 11, 2013. Date of publication May 13, 2013; date of current version May 31, 2013.

The authors are with the Microwave Electronics Laboratory, Department of Microtechnology and Nanoscience, Chalmers University of Technology, SE 412 96 Göteborg, Sweden (e-mail: vessen.vassilev@chalmers.se).

Color versions of one or more of the figures in this paper are available online at http://ieeexplore.ieee.org.

Digital Object Identifier 10.1109/TMTT.2013.2259250

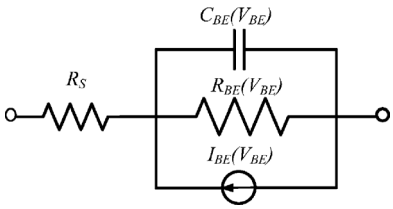

Fig. 1. Simplified equivalent circuit of the base-emitter junction.

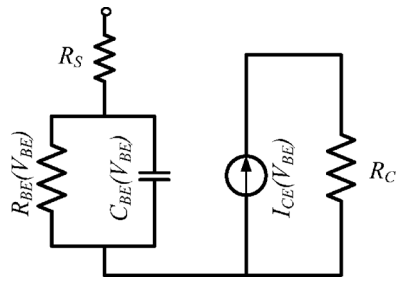

Fig. 2. Equivalent circuit of the DHBT active detector.

II. Responsivity

Responsivity for two types of detectors is considered: a passive detector where a diode is used as a detecting component and a transistor-based active detector.

A. Passive Detector

A power detector is a device that produces dc voltage or current proportional to the input RF power. Responsivity is given as either voltage or current and is defined as

$$R_V = \frac{V_{\rm DC}}{P_{\rm RF}}\ [\rm V/W] \quad R_I = \frac{I_{\rm DC}}{P_{\rm RF}}\ [\rm A/W]. \tag{1}$$

To calculate the upper limit of detector-responsivity at a particular RF frequency, one needs the IVC of the diode, the parasitic series resistance R_S, and the diode capacitance C_{BE}. An equivalent circuit of the base-emitter junction is shown in Fig. 1.

The calculation is based on the Taylor expansion of the diode's IVC around its operating point V_0 and shown as

$$\begin{aligned} i(V_0) =& i(V_0) + \frac{di}{dv}(v - V_0) + \frac{1}{2}\frac{d^2i}{dv^2}(v - V_0)^2 \\ &+ \frac{1}{6}\frac{d^3i}{dv^3}(v - V_0)^3 + \frac{1}{24}\frac{d^4i}{dv^4}(v - V_0)^4 + \cdots \end{aligned} \tag{2}$$

If the applied voltage is $v = A\cos(\omega t)$, the terms producing a dc component in the current are the first, the square, and the quadratic terms. The only term that produces a dc current component proportional to the voltage square (power) for a zero bias voltage is

$$i(v) = \frac{1}{2}\frac{d^2i}{dv^2}v^2. \tag{3}$$

The power absorbed by the junction is

$$P_{\rm RF} = \frac{v^2}{R_{BE}} \tag{4}$$

where $R_{BE} = di/dV$ is the diode differential resistance at the corresponding bias point of the IVC. The current responsivity is thus the ratio of the dc current component and the absorbed RF power and is given by

$$R_I^{\rm MAX} = \frac{i(v)}{P_{\rm RF}} = \frac{1}{2}\frac{d^2i}{dv^2}R_{BE} = \frac{1}{2}\frac{\dfrac{d^2i}{dv^2}}{\dfrac{di}{dv}}. \tag{5}$$

The ratio of the second to the first current derivative in (5) is often called "curvature."

In most cases, the value measured at dc is voltage and the voltage responsivity R_V is thus of interest. The voltage responsivity can be obtained from R_I by multiplying it with the diode resistance R_{BE} at the corresponding bias point of the IVC as

$$R_V^{\rm MAX} = R_I^{\rm MAX} \cdot R_{BE} = \frac{R_I^{\rm MAX}}{di/dv} = \frac{1}{2}\frac{\dfrac{d^2i}{dv^2}}{\left(\dfrac{di}{dv}\right)^2}. \tag{6}$$

The voltage responsivity is sometimes given as

$$R_V^{\rm MAX} = -\frac{1}{2}\frac{\dfrac{d^2v}{di^2}}{\dfrac{dv}{di}}. \tag{7}$$

It can be shown that, for a quadratic function $i = v^2$, (6) and (7) are identical. Note that, in the above expression, R_S and C_{BE} are ignored, and their presence will scale the maximum responsivity at high frequencies with a scaling factor according to [13]

$$C_R = \frac{1}{\left(1 + \dfrac{R_S}{R_{BE}}\right)^2}\frac{1}{1 + \dfrac{R_S}{R_S + R_{BE}} \cdot \dfrac{R_{BE}^2}{1/\omega^2 C_{BE}^2}}. \tag{8}$$

The real voltage responsivity of the detector at high frequencies is the scaled $R_V^{\rm MAX}$ from (6) and shown as

$$R_V = \frac{1}{2}\frac{\dfrac{d^2i}{dv^2}}{\left(\dfrac{di}{dv}\right)^2}C_R. \tag{9}$$

The input parameters needed to predict the responsivity and the optimum bias point at high frequencies are thus the IVC, $C_{BE}(V_{BE})$, and R_S.

B. Active Detector

In this case, a transistor is biased as a current amplifier according to Fig. 2. The RF is applied at the base-emitter whereas the dc component of the collector current is the measure of the RF power.

In this case, the quadratic term in the Taylor expansion $i_C = f(v_{BE})$ is used to derive the responsivity. The analysis of the expected responsivity for the active detector is similar to the one

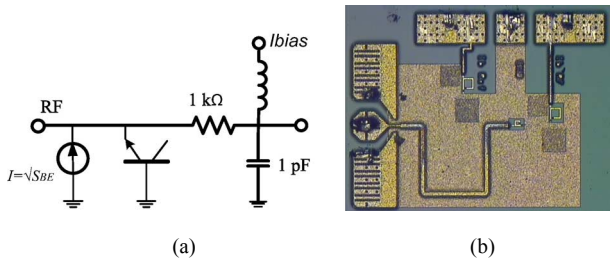

Fig. 3. (a) Simplified schematic of the diode detector not including matching and biasing circuits. A bias-dependent noise current source is used to add the effect of the flicker noise contribution, which is not accounted for in the transistor model. (b) Layout of the circuit. The size of the MMIC is 650/450 μm.

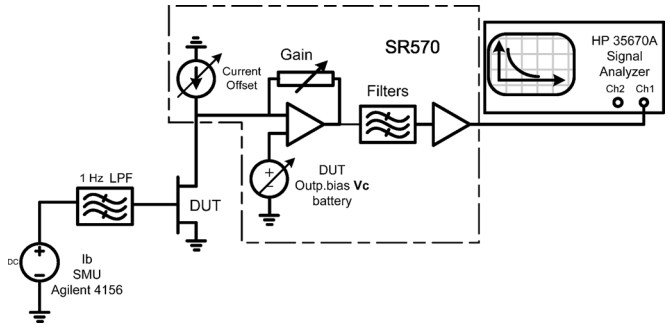

Fig. 4. Setup used to measure the noise current spectrum S_{CE}.

presented above except that the base current is replaced by I_c or βI_b, where β is the dc current gain, and shown as

$$R_V = \frac{1}{2}\frac{\dfrac{d^2 i_c}{dv_{BE}^2}}{\dfrac{di_b}{dv_{BE}}} R_C C_R. \tag{10}$$

The direct consequence of this is that the curvature of the active detector is β times higher than the corresponding curvature of the passive detector. The responsivity at high frequencies is the product of R_V^{MAX} and the scaling factor from (8). The expected R_V, however, is not β times higher, and this will be explained in Section VII, where responsivity of both circuits are compared for transistors with the same size and for $R_C = R_{BE}$.

III. Technology Overview

The circuits are implemented using the Teledyne foundry InP–InGaAs–InP DHBT process. (TSC250). Devices in the technology offer typical RF figures of merit (ft and $f\max$) of 350/600 GHz while maintaining a common-emitter breakdown voltage (V_{CEO}) of greater than 4 V. The DHBT process includes thin-film resistor (50 Ω/sq), a metal–insulator–metal (MIM) capacitor, and four metal layers (M1–M4). The first layer (M1) contacts the transistor and resistor terminals. MIM capacitors are formed with a 200-nm SiN dielectric between M1 and the capacitor metal layer. Three additional interconnect layers are added with 2 μm of interlayer BCB dielectric separating the layers. The top metal layer (M4) is 3 μm to facilitate the formation of a low-loss thin-film microstrip line and to accommodate higher current density requirements.

A scalable Agilent encoded model is available based on on-wafer S-parameter characterization up to 67 GHz. However, the model does not consider low-frequency noise. More details of the process can be found in [17].

IV. Noise Voltage, Responsivity, and NEP of a Passive Detector

The passive detector is implemented by using the BE junction of a DHBT with sizes 0.25 × 2 μm. A thin-film resistor of 1 kΩ is used to isolate RF leakage towards the dc port of the detector. The collector is kept open, as shown in Fig. 3.

The flicker noise is not implemented in the transistor model included in the TSC design kit. The modeling of the flicker noise presented below is based on measurement of the collector current-noise spectrum density carried out with the setup illustrated in Fig. 4. The noise parameters Kf and Af are extracted from noise spectrum measurements at the collector port of the transistor at low frequencies:

$$S_{CE}(f) = Kf\frac{(\beta I_b)^{Af}}{f}. \tag{11}$$

The fitted and measured noise spectra are presented in Fig. 5. The extracted noise coefficients are assumed to be the same for both collector and base terminals and are thus used to define a noise current at the base-emitter junction of the transistor as

$$I = \sqrt{S_{BE}(f)} = \sqrt{Kf\frac{I_b^{Af}}{f}}. \tag{12}$$

The noise current is defined conveniently in a circuit simulator using a bias-dependent noise current source, where the inputs to the source are the measured coefficients and the dc current through the base-emitter junction.

Measurements of the noise current spectrum are performed conveniently at the collector terminal where the collector-emitter impedance is relatively high and independent of the base current. The noise current spectrum S_{CE} was measured for base currents $I_{\mathrm{b}} = 5, 10, 15, 20$ and 30 μA and $\mathrm{Vce} = 1.75$ V using the measurement setup illustrated in Fig. 4. The base current is applied through a 1 Hz filter with large output impedance, which eliminates the noise from the bias source and prevents the noise voltage across the base from being shorted out. The device output is directly connected to a low noise current amplifier with input impedance of 1 Ω. The amplifier also provides a voltage supply used to bias the device output.

The measured and fitted noise spectrum for a 0.25 × 2 μm DHBT are depicted in Fig. 5. The expected noise-current spectral density at the base is shown in Fig. 6.

The expected noise voltage of the detector at frequencies dominated by the flicker noise is the product of the square root of the flicker current noise spectrum at the BE junction (12) and the junction resistance *dv/di* at the specific bias point, in this case 1 kΩ for $I_b = 30$ μA. The simulated and the measured noise voltage at the output of the detector are presented in Fig. 7.

The upper limit of responsivity obtainable from a 0.25 × 2 μm DHBT was derived in Section II and is calculated in Section VII to be 8 kV/W. An HB simulation is

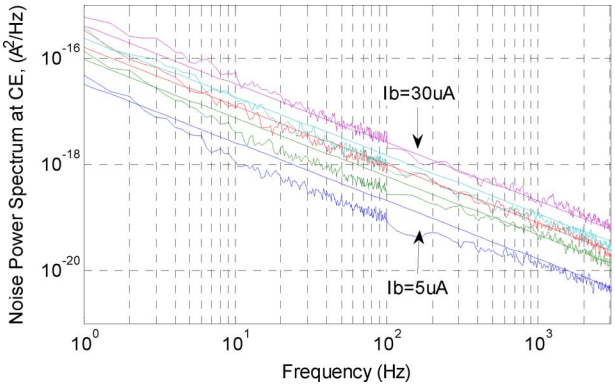

Fig. 5. Measured and modeled noise current spectrum of the 0.25×2 μm DHBT $I_b = 5$, 10, 15, 20, and 30 μA. The extracted noise coefficients are: $Kf = 8e-13$; $Af = 1$.

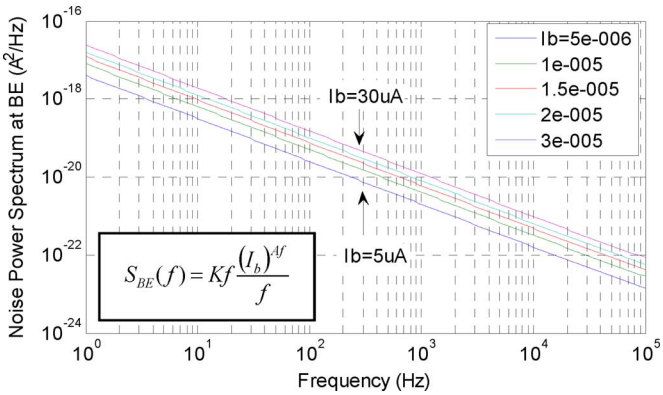

Fig. 6. Expected noise current density at the base calculated from the measured Kf and Af at the collector.

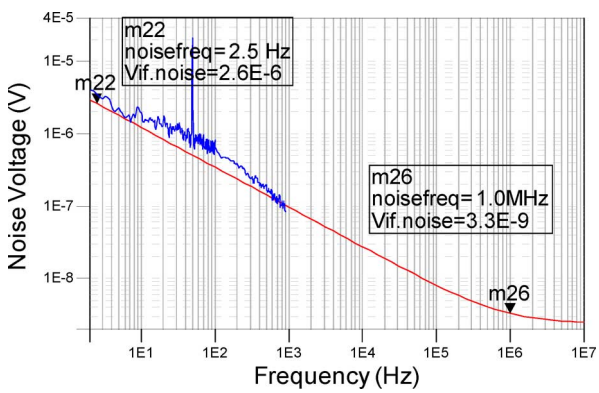

Fig. 7. Measured and simulated noise voltage of the detector. A bias-dependent noise current source at the BE was used in ADS together with the extracted noise coefficients to account for the flicker noise.

used to predict the responsivity of the particular detector circuit shown in Fig. 3. The simulation predicts a R_V of 3.4 kV/W and includes losses in the matching circuit and the effect of the 1-kΩ resistor. The matching circuit was designed to deliver a return loss (RL) greater than 10 dB over the frequency range 165–220 GHz. However, the measured RL is greater than 10 dB over 145–180 GHz.

For the responsivity measurement, a pulse-modulated RF is applied at the detector input using an X6 multiplier fed by a synthesizer. The modulation signal, which is rectangular pulse

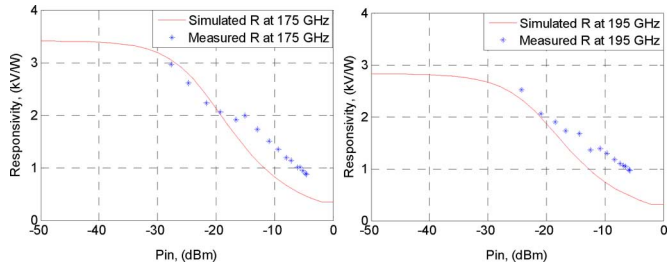

Fig. 8. Simulated and measured responsivity. Due to difficulties in measurement of low power levels, the responsivity is measured at RF power levels above -28 dBm where the detector is in saturation.

series with frequency of several kilohertz, is also used to synchronize a lock-in amplifier that measures the detected voltage. An attenuator is used to vary the RF power at the input of the detector, and responsivity is calculated for each power level. Due to the lack of a precision attenuator, the RF power is measured for each attenuator position using an Erickson power meter.[1] It is difficult to measure power levels less than 1 μW with sufficient accuracy, and, therefore, the responsivity measurements are performed for input power levels not less than -28 dBm. The simulated and measured responsivities are plotted in Fig. 8.

The NEP is defined as *the noise power at the input of the detector that produces SNR at the output equal to one*. In other words, the NEP is the input signal power that produces detected voltage equal to the measured noise-voltage Vn. In this work, the NEP is calculated from measurements of Vn at the output of the detector and thus is related to the bandwidth over which Vn is measured. To make possible comparison between detectors, Vn is measured over a bandwidth of 1 Hz, and its value is given in units of V/$\sqrt{\text{Hz}}$. Because of the presence of $1/f$ noise, it is useful to present the NEP for a specific video frequency. The NEP is calculated as

$$\text{NEP} = \frac{V_n}{R_V}\ [\text{W}/\sqrt{\text{Hz}}]. \tag{13}$$

Based on the measured/modeled noise voltage from Fig. 7 and measured R_V, the NEP versus video frequency can be calculated and is presented in Fig. 9.

V. Noise Voltage, Responsivity, and NEP of an Active Detector

The active detector uses a 0.25×3 μm transistor in a configuration as shown in Fig. 10. The base current is 16 μA and Ic is 343 μA. As in the case with the passive detector, the flicker noise is modeled in ADS with the help of a bias-dependent noise current source connected at the collector and with coefficients extracted from noise spectrum measurements of the transistor at low frequencies. The current–noise spectrum is measured at several I_b, and the Kf and Af coefficients are extracted so that they match well with all values of the base/collector currents.

The measured and fitted noise-current spectral densities of a 0.25×3 μm DHBT at the collector terminal are depicted in Fig. 11. Due to the high collector-emitter resistance, the output noise voltage Vn is calculated by the product of $(S_{CE}^{0.5}) * Rc$.

[1][Online]. Available: http://vadiodes.com/

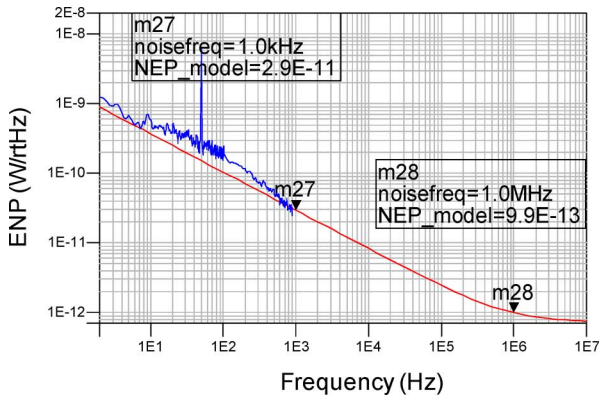

Fig. 9. Expected and measured NEPs of the diode detector; responsivity of 3300 is considered.

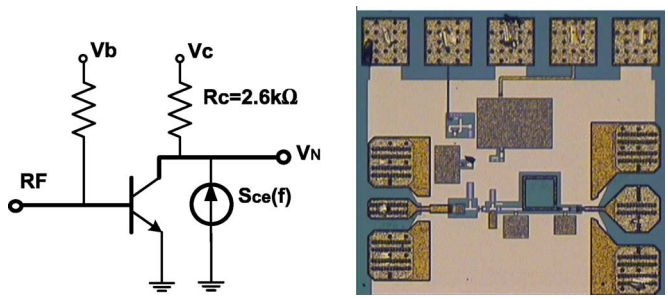

(a) (b)

Fig. 10. (a) Simplified schematic of the active detector not including matching circuitry. (b) Layout of the circuit. The size of the MMIC is 480/440 μm.

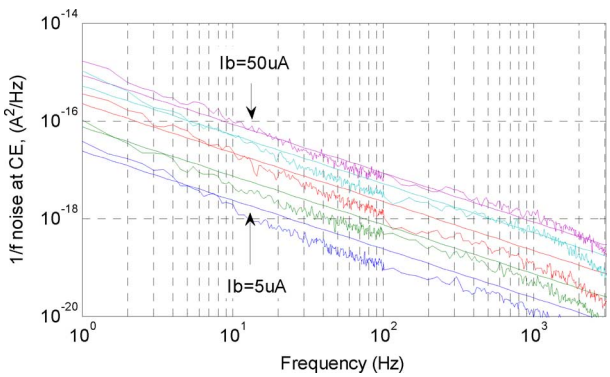

Fig. 11. Measured and modeled noise–current spectrum $S_{CE}(f)$ of 3 μm DHBT for $V_C = 1.75$ V and $Ib = 5, 10, 20, 35$, and 50 μA. The extracted coefficients are $Kf = 12e-13$, $Af = 1.03$.

The modeled noise voltage is compared with the measured one in Fig. 12.

The upper limit of the responsivity calculated by (10) for the 0.25×3 μm HBT and $Rc = 2.6$ kΩ is 55 kV/W. The HB calculated responsivity for the real circuit is compared with measurements in the figure below.

Based on the measured/modeled noise voltage from Fig. 12 and measured responsivity, the NEP versusvideo frequency can be calculated and is presented in Fig. 14.

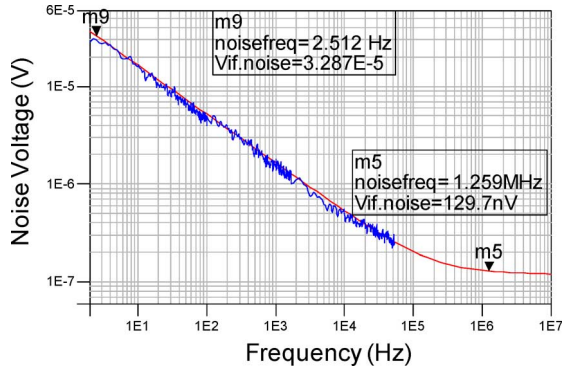

Fig. 12. Measured and modeled noise voltage of the active detector versus video frequency for $Ib = 20$ μA, $Ic = 450$ μA, and $R_C = 2.6$ kΩ.

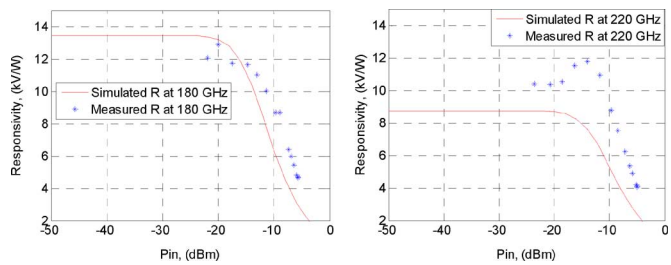

Fig. 13. Simulated (using HB) and measured responsivities of an active detector with 0.25×3 μm DHBT, $Ib = 20$ μA, $Ic = 450$ μA, and $Rc = 2.6$ kΩ.

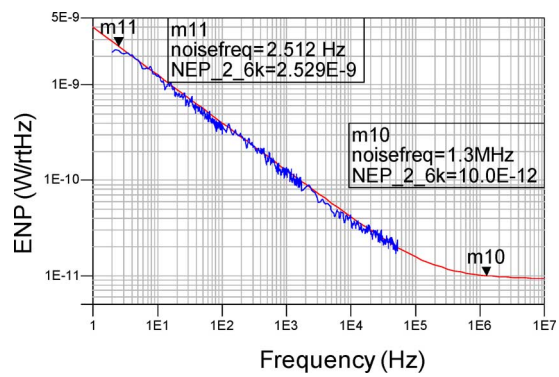

Fig. 14. Expected and measured NEPs of the active detector versus video frequency for $Ib = 20$ μA and $Ic = 450$ μA. Responsivity of 13400 is considered.

VI. Noise Voltages—Active Versus Passive

The expected noise voltages for the active and the passive detectors are

$$V_N^{\text{Active}} = \sqrt{S_{CE}} \cdot R_C \quad V_N^{\text{Passive}} = \sqrt{S_{BE}} \cdot R_{BE}. \tag{14}$$

Since the coefficients Kf and Af are almost the same for both DHBT sizes, they can cancel and the ratio of the measured noise voltages is

$$\frac{V_N^{\text{Active}}}{V_N^{\text{Passive}}} = \sqrt{\beta} \cdot \frac{R_C}{R_{BE}} = 2.6 \cdot \sqrt{20} = 11.6. \tag{15}$$

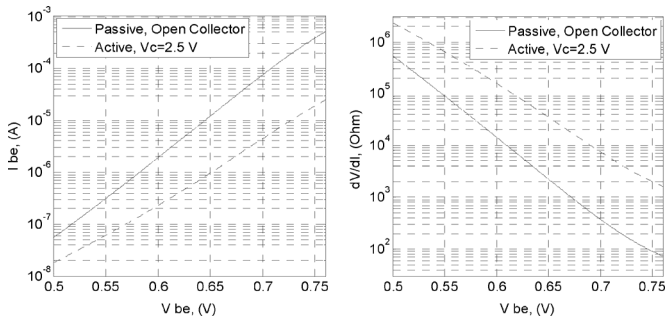

(a) (b)

Fig. 15. Comparison of a 2-μm DHBT with open collector and with collector biased with 2.5 V through a 2.5-kΩ resistor. (a) IVC for the base-emitter junction. (b) Base-emitter resistance for both cases.

Indeed, looking at the measured data from Figs. 7 and 12, for a frequency of 2.5 Hz, we have $Vn^{\mathrm{Active}} = 33\ \mu$V and $Vn^{\mathrm{Passive}} = 3\ \mu$V, resulting in a ratio of 11.

VII. Responsivity—Active Versus Passive

It was shown that the noise voltage of an active detector is $\sqrt{\beta}$ times higher than the noise voltage of a passive detector provided that $R_C = R_{BE}$, where R_{BE} is the resistance of the passive detector dV_{BE}/dI_b at the optimum bias point, typically 1–2 kΩ. The current responsivity of the active detector is β times higher than the corresponding responsivity for the passive detector, and one would expect that the voltage responsivity of the active detector is again β times higher for $R_C = R_{BE}$. However, the active detector cannot deliver this responsivity for a reason related to difference in the base-emitter IVCs between the detectors.

Fig. 15 shows base-emitter IVC and junction resistance for both detectors: passive (when the collector is open, or connected to the base) and active when the collector is biased. It can be seen from the figure that in the case of active detector, a higher V_{BE} is required to achieve certain I_b, or junction resistance. The scaling factor accounting for the junction capacitance and series resistance is given in (8), where C_{BE} and R_{BE} are bias-dependent. This scaling factor will have a peak value at specific V_{BE} such that $R_{BE} = Xc = 1/(\omega C_{BE})$. The peak value of the scaling factor, as calculated by (8) and shown in Fig. 16, differs dramatically between the passive and the active detectors. In the case of active detector (three-terminal case), the device is operating as a forward-biased HBT and the injected emitter current is going through the collector terminal. In this case the base current is just the base-recombination current determined by the transistor current gain β. In the two-terminal (passive detector) case, there is no collector current flow and the injected emitter current must all go through the base terminal, and therefore the base current is β times higher than in the active case. As result, the $I_b(V_{BE})$ characteristic shifts towards higher base-emitter voltages for the active detector where a higher V_{BE} is required to achieve certain I_b or R_{BE}. The maximum in the scaling factor will also shift towards higher voltages where C_{BE} is higher, resulting in reduced responsivity.

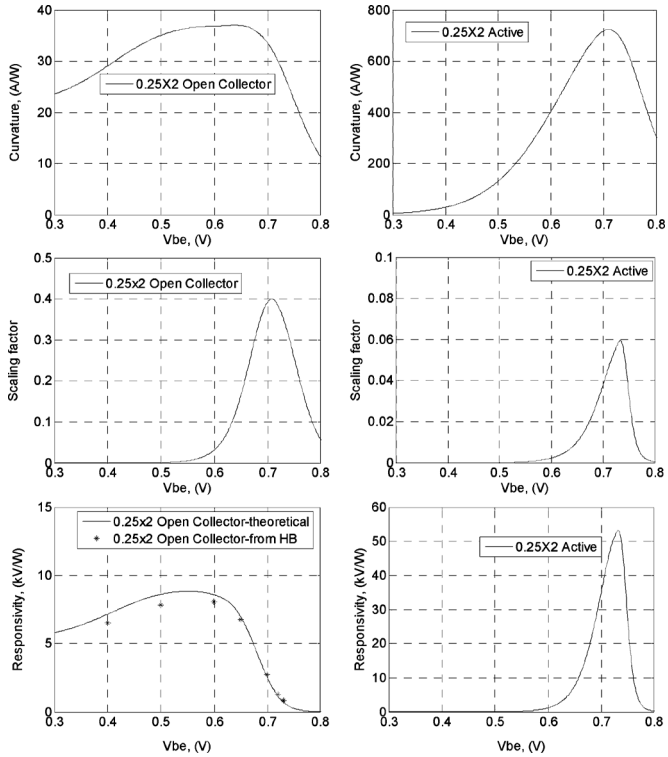

Fig. 16. Curvature, scaling factor from (8), and predicted R_V of a 2-μm passive (left) compared with an active detector. As can be noticed, the current responsivity of the active detector is β times higher than in the case of passive, but not the R_V.

As shown in (9), R_V is proportional to the product of curvature and the scaling factor C_R. The responsivity of the active detector is expected to be

$$R_V^{\mathrm{Active}} = R_V^{\mathrm{Passive}} \beta \frac{R_C}{R_{BE}^{\mathrm{Passive}}}. \tag{16}$$

The calculations for the active detector presented in Fig. 16 are for $Rc = 2.6\mathrm{k}\Omega$, the responsivity is compared with the passive detector for bias of $Vbe = 0.644$ V, where R_{BE} has the same value. The unscaled maximum responsivity for the active detector is expected to be

$$R_V^{\mathrm{Active}} = R_V^{\mathrm{Passive}} \cdot \beta = 7317 \cdot 20 = 146.3\ [\mathrm{kV/W}].$$

However, because of the lower value in the scaling factor for the active detector due to *Rs* and *Cj*, the responsivity is reduced to

$$R_V^{\mathrm{Active}} = R_V^{\mathrm{Passive}} \cdot \beta = 7317 \cdot 20 \cdot \frac{0.056}{0.14} = 58.5\ [\mathrm{kV/W}] \tag{18}$$

which is also the value presented in Fig. 16.

VIII. Detection of Thermal Noise

In the case of thermal noise, the detector measures the noise temperature of its input termination. The resolution in temperature ΔT that the detector can deliver can be thought of as the temperature at the input of the detector that produces voltage change at the output equal to the noise voltage. This delta change

TABLE I
MEASURED VALUES OF NEP AT VIDEO FREQUENCIES AT 1 KHZ AND ABOVE THE CORNER FREQUENCY. THE VALUES ARE COMPARED TO SIGE W- AND D-BAND DETECTORS REPORTED IN [2] AND [3]

	RF freq *GHz*	Flicker noise corner freq	NEP at 1kHz, *pW/√Hz*	NEP above Corner freq *pW/√Hz*
Passive	180	1 MHz	30	1.9
Active	180	1 MHz	110	10
[2]	94	10 kHz	8	3.5
[3]	165	160 Hz	6	6

in temperature corresponds to a change in the power of $\mathrm{NEP}\cdot\sqrt{B_V}$, where $B_v = f_v^{\mathrm{Max}} - f_v^{\mathrm{Min}}$ is the video bandwidth. The maximum video frequency f_v^{Max} is inversely proportional to the integration time τ, whereas the minimum video frequency f_v^{Min} is related to how often the radiomoeter is calibrated. The choice of video bandwidth is a part of the system design and depends on the type of radiometer and the application. To avoid the effect of $1/f$ gain fluctuations, the f_v^{Max} needs be higher than the corner frequency indicated in the NEP noise spectrum from Figs. 9 and 14.

The NEP plots from Figs. 9 and 14 are sufficient to evaluate the usefulness of the detector for the specific application and method for gain drift compensation. One way to calculate the temperature resolution is given by

$$P_N = \mathrm{NEP}\sqrt{B_v} = k\cdot\Delta T\cdot B_{\mathrm{RF}}$$
$$\Delta T = \frac{\mathrm{NEP}\sqrt{B_v}}{k\cdot B_{\mathrm{RF}}}\ [\mathrm{K}] \tag{19}$$

which requires integration of the NEP over the video bandwidth. This can be done analytically by fitting a line to the NEP plot. An example of ΔT calculation is presented in [1].

Table I presents an NEP comparison between the detectors presented in this paper and detectors based on SiGe technology.

To improve the resolution of the system, an LNA is needed in front of the detector. The LNA will scale ΔT from (19) with the inverse of its gain. The gain of the LNA preceding the mixer is limited by the linearity of the detector, which is the maximum power that the detector can convert to a voltage and still be linear. Therefore detector saturation power is also an important figure of merit. Referring to Fig. 8 for a passive detector, the responsivity remains constant for RF power below 1 μW. Considering a certain RF bandwidth, LNA noise temperature and scene temperature T_{BG}, the maximum allowable gain is

$$G_{\mathrm{LNA}} = \frac{1[\mu\mathrm{W}]}{k\cdot(T_{\mathrm{LNA}} + T_{BG})\cdot B_{\mathrm{RF}}}. \tag{20}$$

For example, for an LNA with a noise figure of 6.5 dB (1000 K), background temperature of 300 K, and RF bandwidth of 30 GHz, the maximum LNA gain is 32 dB (1800). Having an LNA with this much gain will make ΔT at the LNA input dominated by the LNA noise. In the case of the active detector, the ΔT of the detector is three times higher than for the passive for the same RF/video bandwidth. However, since the saturation level of the active detector is 10 dB higher than the passive, it allows for extra gain in the LNA.

IX. CONCLUSION

This paper presents measurement results of responsivity and NEP of two types of detectors, a passive type where the BE junction of a 0.25×2 μm DHBT is used as a diode rectifier, and an active type where a 0.25×3 μm DHBT is used as an active rectifier with β times higher output current. To model the noise at low frequencies, measurements of noise power spectrum were carried out, and flicker noise coefficients were extracted. Measured noise voltages and NEP are compared with modeled ones. The NEP presented in this paper is not as good as the NEP demonstrated earlier using SiGe technology for frequencies below 200 GHz, but it may become advantageous at higher frequencies (above 200 GHz), especially when the detector is integrated with an LNA.

The voltage responsivity of the active detector is proportional to R_C, however the noise voltage is also proportional to R_C and therefore higher values of collector resistance result in no improvement in the NEP. Compared with a passive detector, the active circuit produces $\sqrt{\beta}$ times higher noise voltage but it cannot deliver the expected β times higher voltage responsivity and therefore may have higher NEP. The active detector shows higher saturation levels, in this case -20 dBm, and therefore can be integrated together with an LNA with higher gain and therefore deliver better temperature resolution.

ACKNOWLEDGMENT

The authors would like to acknowledge M. Urteaga, Teledyne Scientific Company, for helping us explain the results presented in Section VII.

REFERENCES

[1] J. J. Lynch, H. P. Moyer, J. H. Schaffner, Y. Royter, M. Sokolich, B. Hughes, Y. J. Yoon, and J. N. Schulman, "Passive millimeter-wave imaging module with preamplified zero-bias detection," *IEEE Trans. Microw. Theory Tech.*, vol. 56, no. 7, pp. 1592–1600, Jul. 2008.

[2] J. W. May and G. M. Rebeiz, "Design and characterization of W-band SiGe RFICs for passive millimeter-wave imaging," *IEEE Trans. Microw. Theory Tech.*, vol. 58, no. 5, pp. 1420–1430, May 2010.

[3] E. Dacquay, A. Tomkins, K. H. K. Yau, E. Laskin, P. Chevalier, A. Chantre, B. Sautreuil, and S. P. Voinigescu, "D-band total power radiometer performance optimization in a SiGe HBT technology," *IEEE Trans. Microw. Theory Tech.*, vol. 60, no. 3, pp. 813–826, Mar. 2012.

[4] L. Gilreath, V. Jain, and P. Heydari, "Design and analysis of a W-band SiGe direct-detection-based passive imaging receiver," *IEEE J. Solid-State Circuits*, vol. 46, pp. 2240–2252, .

[5] R. Neidert and S. Binari, "Millimeter-wave planar InP Schottky diodes and their small-signal equivalent circuit," *IEEE Trans. Microw. Theory Tech.*, vol. 37, no. 11, pp. 1694–1698, Nov. 1989.

[6] H. Kazemi, G. Nagy, L. Tran, E. Grossman, E. R. Brown, A. C. Gossard, G. D. Boreman, B. Lail, A. C. Young, and J. D. Zimmerman, "Ultra sensitive ErAs/InAlGaAs direct detectors for millimeter wave and THz imaging applications," in *IEEE MTT-S Int. Microw. Symp. Dig.*, 2007, pp. 1367–1370.

[7] J. Hesler and T. Crowe, "Responsivity and noise measurements of zero-bias Schottky diode detectors," in *Proc. 18th Int. Symp. Space Terahertz Technol.*, Pasadena, CA, USA, Mar. 2007, pp. 89–92.

[8] W. Gabriel, "Tunnel-diode low-level detection," *IEEE Trans. Microw. Theory and Tech.*, vol. MTT-15, no. 10, pp. 538–553, Oct. 1967.

[9] HRL Laboratories, LLC. Malibu, CA, 3011 Malibu Canyon Road, 90265-4797.

[10] K. Sengupta, D. Seo, and A. Hajimiri, "A Terahertz imaging receiver in 0.13 μm SiGe BiCMOS technology," in *Proc. 36th Int. Conf. Infrared, Millimeter Terahertz Waves*, 2011.

[11] A. Lisauskas, U. Pfeiffer, E. Öjefors, P. H. Bolìvar, D. Glaab, and H. G. Roskos, "Rational design of high-responsivity detectors of terahertz radiation based on distributed self-mixing in silicon field-effect transistors," *J. Appl. Phys.*, vol. 105, pp. 1–7, Jun. 2009.
[12] A. Lisauskas, W. von Spiegel, S. Boubanga-Tombet, A. El Fatimy, D. Coquillat, F. Teppe, N. Dyakonova, W. Knap, and H. G. Roskos, "Terahertz imaging with GaAs field-effect transistors," *Electron. Lett.*, vol. 44, no. 6, Mar. 2008.
[13] H. C. Torrey and C. A. Whitmer, "Crystal rectifiers," *MIT Rad. Lab. Series*, vol. 15, 1948.
[14] T. Lee, J. East, C. Chen-Yu, G. Rebeiz, R. Dengler, I. Mehdi, P. Siegel, and G. Haddad, "The fabrication and performance of planar doped barrier diodes as 200 GHz subharmonically pumped mixers," *IEEE Trans. Microw. Theory Tech.*, vol. 42, no. 4, pp. 742–749, Apr. 1993.
[15] Teledyne Scientific Company, 1049 Camino Dos Rios. Thousand Oaks, CA, 91360.
[16] L. Gilreath, V. Jain, and P. Heydari, "Design and analysis of a W-band SiGe direct-detection-based passive imaging receiver," *IEEE J. Solid-State Circuits*, vol. 46, no. 10, pp. 2240–2252, Oct. 2011.
[17] M. Urteaga, M. Seo, J. Hacker, Z. Griffith, A. Young, R. Pierson, P. Rowell, A. Skalare, and M. J. W. Rodwell, "InP HBT integrated circuit technology for terahertz frequencies," in *Proc. IEEE Compound Semicond. Integr. Circuit Symp.*, Oct. 2010, pp. 1–4.

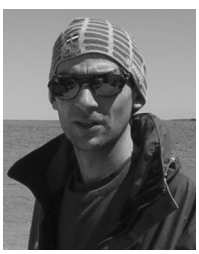

Vessen Vassilev received the M.Sc. degree in radio communications from the Sofia Technical University, Sofia, Bulgaria, in 1995, and the M.Sc. degree in digital communications and Ph.D. degree in radio and space science from Chalmers University of Technology, Göteborg, Sweden, in 1998 and 2003, respectively.

Between 1998 and 2008, he was working with the development of millimeter-wave receivers for applications in radio astronomy and space sciences. Instruments designed by him are currently in operation at the Atacama Pathfinder Experiment (APEX) telescope and at the Onsala Space Observatory. Since 2008, he has been with the Microwave Electronics Laboratory, Department of Microtechnology and Nanoscience, Chalmers University of Technology, Göteborg, Sweden. His current interests are in the development millimeter-wavelength sensors based on monolithic microwave integrated circuit technologies.

Herbert Zirath (F'11) received the M.Sc. and Ph.D. degrees from Chalmers University of Technology, Göteborg, Sweden, in 1980 and 1986, respectively.

Since 1996, he has been a Professor of high-speed electronics with the Department of Microtechnology and Nanoscience, MC2, Chalmers University of Technology, Göteborg, Sweden, where, In 2001, he became the Head of the Microwave Electronics Laboratory. He currently leads a group of approximately 50 researchers in the area of high-frequency semiconductor devices and circuits. His main research interests include foundry-related MMIC designs for millimeter-wave applications based on both III–V and silicon devices, SiC- and GaN-based transistors and circuits for high-power applications, device modeling including noise and large-signal models for FET and bipolar devices, and InP-HEMT devices and circuits. He has authored or coauthored over 500 refereed journal/conference papers. He holds six patents.

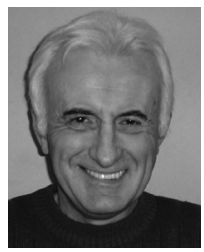

Rumen Kozhuharov was born in Sofia, Bulgaria. He received the B.S. and M.S. degrees in electronic engineering from the Institute of Mechanical and Electrical Engineering, Sofia, Bulgaria, in 1972, and the Ph.D. degree in physics from the Institute of Electronics, Bulgarian Academy of Sciences, Sofia, Bulgaria, in 1977.

He was a Research Associate with the Institute of Electronics—Sofia and has been involved with the design and development of transceivers, used for environmental tests of radio relay stations. Since 2000, he has been with the Department of Microtechnology and Nanoscience (MC2), Chalmers University of Technology, Göteborg, Sweden, where he is involved in the design and investigation of low-noise hybrid oscillators, stabilized with DR and HTSC resonators, monolithic microwave integrated circuit millimeter-wave voltage-controlled oscillators and multipliers for high-data-rate communication links. He has authored and coauthored more then 75 papers in international journals and conference proceedings and one book and holds one patent.

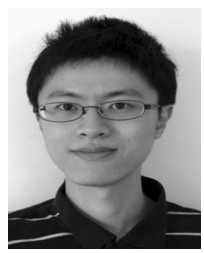

Szhau Lai (S'12) was born in Taoyuan, Taiwan, in 1985. He received the B.S. degree in electrical engineering from the National Chiao-Tung University, Taiwan, in 2008, and the M.S. degree in electrical engineering from Chalmers University of technology, Göteborg, Sweden, in 2009, where he is currently working toward the Ph.D. degree in microtechnology and nanoscience.

His research interest includes the design of voltage-controlled oscillators (VCOs), noise modeling, and VCO phase-noise analysis.

Mr. Lai won the transistor modeling competition at the 2012 IEEE Microwave Theory and Techniques Society (IEEE MTT-S) International Microwave Symposium.